Nanoscale

Accepted Manuscript

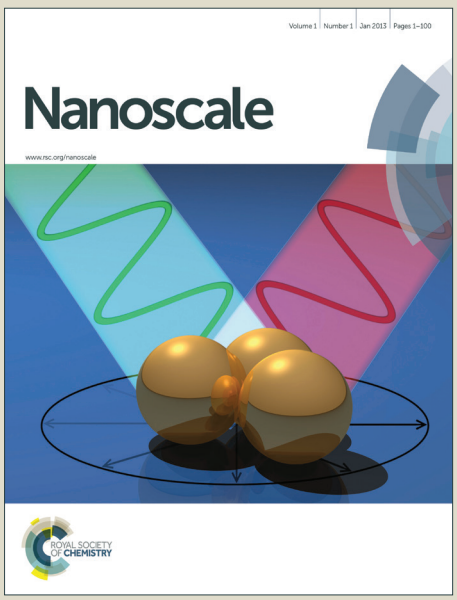

ROYAL SOCIETY OF CHEMISTRY

www.rsc.org/nanoscale

Table of contents

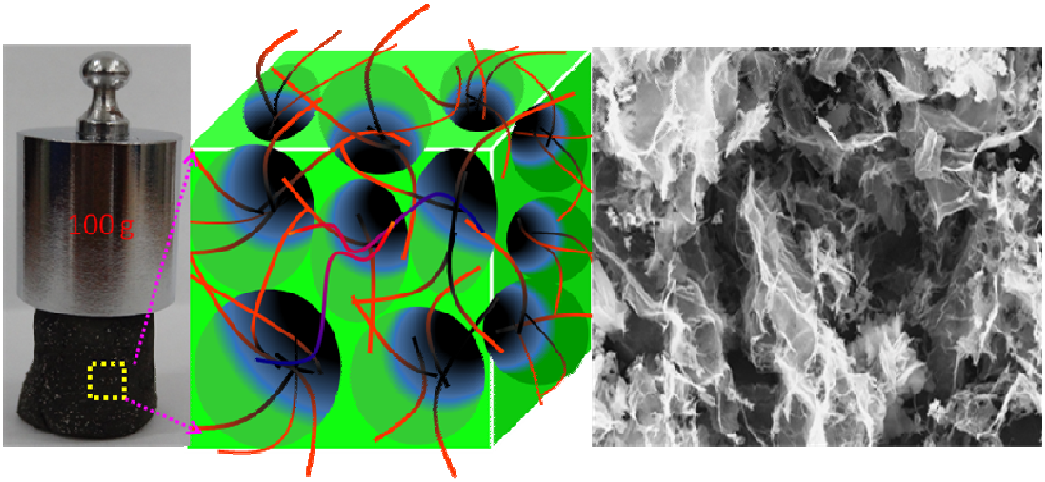

3D porous $AgVO_3$ nanowires/graphene composite aerogels show high electrical conductivity, mechanical flexibility, and good electrochemical performance for lithium ion storage.

Nanoscale

RSCPublishing

COMMUNICATION

1-Dimensional $AgVO_3$ Nanowires Hybrid with 2-Dimensional Graphene Nanosheets to Create 3-Dimensional Composite Aerogels and its Improved Electrochemical Property

Cite this: DOI:10.1039/x0xx00000x

Liying Liang,[b,c] Yimeng Xu,[b] Yong Lei[c]* and Haimei Liu[a,b]*

Received Xth XXXXXXXXX 20XX,
Accepted Xth XXXXXXXXX 20XX

DOI: 10.1039/x0xx00000x

www.rsc.org/nanoscale

Three-Dimensional (3D) porous composite aerogels have been synthesized *via* an innovative *in situ* hydrothermal method assisted by freeze-drying process. In this hybrid structure, one-dimensional (1D) $AgVO_3$ nanowires are uniformly dispersed on two-dimensional (2D) graphene nanosheets surfaces and/or are penetrated through the graphene sheets, forming 3D porous composite aerogels. As cathode materials for lithium-ion batteries, the composite aerogels exhibit high discharge capacity, excellent rate capability, and good cycling stability.

To date, new carbon materials have attracted extensive attention, such as carbon nanorings[1], graphene paper[2], graphene fibers[3], carbon aerogels[4]. Among these, graphene aerogels, a typical kind of three-dimensional (3D) macroscopic assembly consisting of the microporous and mesoporous frameworks that prevent the restacking of graphene sheets, are particularly notable in recent two years. 3D graphene aerogels show light weight, high conductivity, large surface area, high mechanical strength, and ample volume with hierarchically porous structure.[5-7] As a result of these unique properties, a great deal of work has been done to study graphene aerogels in various technological fields including electrocatalysis, water treatment, and supercapacitors.[8,9]

Recently, there have some progresses concerning the assembly of zero-dimensional (0D) nanosized particles on 3D graphene aerogels network. For example, 3D N-doped graphene aerogel-supported monolithic Fe_3O_4 nanoparticles can be used as efficient cathode catalysts for the oxygen reduction.[10] Moreover, $MnCO_3$/graphene hydrogel composite prepared by a hydrothermal process present a high specific capacitance for supercapacitor electrode applications.[11] This unique 3D structure allows most of the graphene sheets to be exposed to electrolyte, and also provides open channels for electrolyte transportation.

However, until now, there are few reports focusing on the assembly of 3D graphene aerogels with one-dimensional (1D) nanostructures (mostly nanowires and nanotubes). It is well known that 1D nanomaterials have much larger surface area comparing to that of 0D nanoparticles. As the electrode materials, we believe that 3D graphene aerogels with deposited 1D nanostructures can offer a continuous electron pathway to ensure good electrical contact and to facilitate ion transport by shortening diffusion pathways. Therefore, an improved electrochemical performance is highly expected to be achieved.

In this communication, by using a facile one-step hydrothermal method assisted by a freeze-drying process, innovative 3D porous composite aerogels with interconnected macroporous networks are *in-situ* fabricated from 1D $AgVO_3$ nanowires with 2D graphene nanosheets. $AgVO_3$, as a cathode active material in lithium primary batteries for implantable medical devices, shows high energy density and long-term stability.[12-14] However, its low electrical conductivity[15-17] and slow Li^+ diffusion rate[17] limit its practical applications. It has been found that $AgVO_3$ in integration with highly electrical conductive carbon materials (*e.g.*, polyaniline, polypyrrole, and carbon nanotubes) can definitely address its poor

[a]*College of Environmental and Chemical Engineering, Shanghai University of Electric Power, Shanghai 200090, PR China*
[b]*State Key Laboratory of Chemical Resource Engineering, Beijing University of Chemical Technology, Beijing 100 029, PR China. E-mail: liuhm@mail.buct.edu.cn*
[c]*Institute for Physics and IMN MacroNano® (ZIK), Ilmenau University of Technology, Ilmenau, 98693, Germany. E-mail: yong.lei@tu-ilmenau.de*
†Electronic Supplementary Information (ESI) available: Preparation, characterization, SEM images, XRD patterns, and XPS of $AgVO_3$/GAs. See DOI: 10.1039/ x0xx00000x

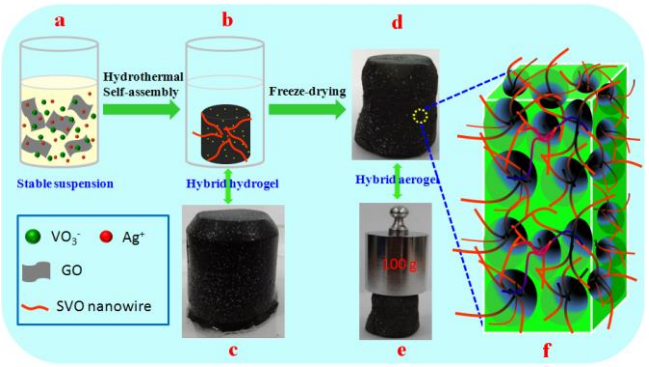

Fig. 1 Schematic illustration for the synthesis of 3D $AgVO_3$/GAs. (a) Stable suspension of precursor in a vessel. (b) Ideal hydrogel assembled model in a vessel. Digital photos of (c) hybrid hydrogel and (d, e) aerogels. (f) Ideal structure model of $AgVO_3$/GAs.

cycling and rate issues that suffer from low electronic conductivity.[18-20] Thereby, we managed to integrate $AgVO_3$ with graphene aerogels to improve its electrochemical properties. When used as cathode materials for lithium-ion batteries (LIBs), $AgVO_3$/graphene composite aerogels ($AgVO_3$/GAs) reveal high discharge capacity, excellent rate capability, and good cycling stability.

The synthesis process of 3D $AgVO_3$/GAs is illustrated in Fig.1. Firstly, graphene oxide (GO) was dispersed in water by sonication, reaching a concentration up to 1.5 mg mL^{-1}. Secondly, $AgNO_3$ and NH_4VO_3 were slowly added to the GO dispersion to form a stable suspension (Fig.1a). Next, the mixture was hydrothermal self-assembly at 180 ℃ for 72 h to generate a 3D macroscopic graphene-based hybrid hydrogel (Fig.1b and 1c). In this way, $AgVO_3$ could nucleate and grow on the graphene surface to form the integrated nanowires, and GO was reduced simultaneously to graphene and self-assembled to construct 3D porous network (Fig. S1). Therefore, it is worth emphasizing that the hydrothermal synthesis method we used guarantees that the two processes, namely, GO reduction to graphene and the decoration of $AgVO_3$ nanowires on the surface of graphene, are implemented in the same step. Finally, the as-prepared hybrid hydrogels were directly dehydrated *via* a freeze-drying process to keep the 3D framework (Fig. 1d). The obtained composite aerogels reveal light weight and excellent apparent mechanical strength (Fig. 1e). One hybrid aerogels with a weight of around 0.94 g can support 100 g weight with little deformation. Fig. 1f is the ideal structure model. In this hybrid structure, 1D $AgVO_3$ nanowires are uniformly dispersed on 2D graphene surfaces and/or are penetrated through the graphene sheets, forming 3D porous composite aerogels. Moreover, the interconnected $AgVO_3$ nanowires are utilized as a spacer to inhibit the aggregation of graphene layers, resulting in a high contact area between the electrolyte/electrode, as well as a bridge for electron transfer between graphene sheets. Graphene offers sufficient electrons for $AgVO_3$ nanowires, leading to enhanced electrical conductivity. The abundant pores facilitate the transportation of the electrolyte ions and electrons into the inner region of the composite aerogels.

The morphology of as-prepared $AgVO_3$/graphene composite aerogels was investigated by scanning electron microscopy (SEM). It is found from Fig. S2 that reaction time plays an important role in forming well-defined $AgVO_3$ nanowires and well-assembled 3D porous hybrid network in the composite aerogels, hence indicating that the best hydrothermal time is 72 h. SEM images of $AgVO_3$/GAs for 72 h (Fig. 2a and 2b) show an interconnected and porous 3D architecture, in which the pore sizes are in the range from submicrometer to several micrometers. The pore walls of the 3D porous structure consist of thin layers of stacked graphene sheets, which are very important for effective electrolyte transport and active-site accessibility. A closed observation of the composite is shown in Fig. 2c and exhibits that $AgVO_3$ nanowires (lengths of several tens of micrometers) are uniformly grown on both sides of graphene in a sandwich-like manner, indicating efficient assembly between $AgVO_3$ nanowires and graphene layers. $AgVO_3$ nanowires have bridged the defects for electron transfer as well as increased the layer spacing between graphene sheets, resulting in improved electrical conductivity of $AgVO_3$ nanowires. The N_2 adsorption-

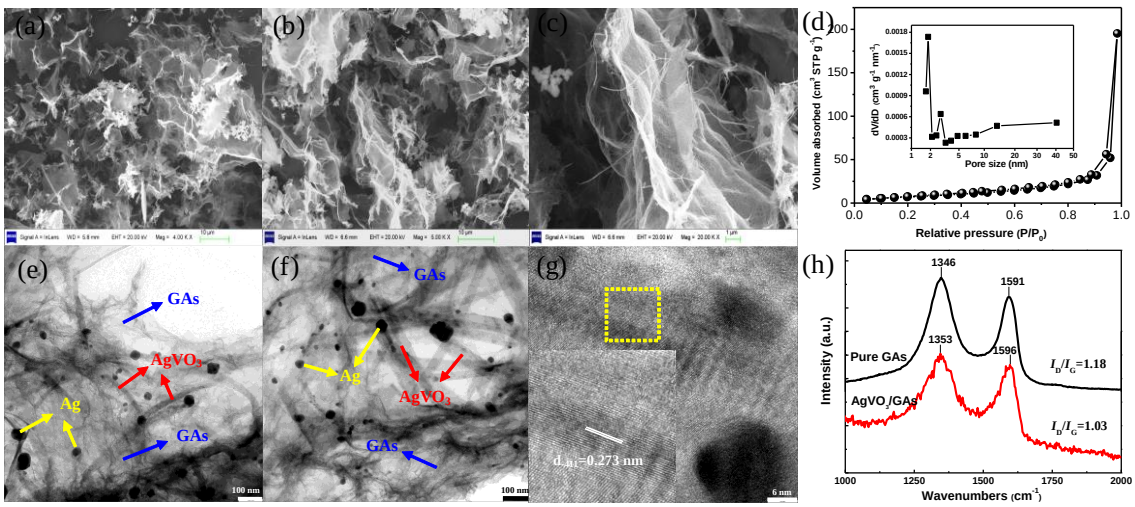

Fig. 2 (a, b, c) SEM images, (d) Nitrogen sorption isotherm and (d inset) pore-size distribution, (e, f) TEM images of $AgVO_3$/GAs. (g) HRTEM image of an individual $AgVO_3$ nanowire. (h) Raman spectra of pure graphene aerogels and $AgVO_3$/GAs.

desorption isotherm of $AgVO_3$/GAs in Fig. 2d shows that it has a surface are of 32.56 m^2 g^{-1} with abundant pores from micropores (~1.8 nm) to mesopores (2.8-40 nm) (the inset in Fig. 2d). It is noticeable that these pores allow most of the graphene sheets to be exposed to electrolyte and provide open channels for electrolyte transport, hence benefiting the electrochemical performance of $AgVO_3$/GAs. TEM images (Fig. 2e and 2f) offer more information about the distribution of $AgVO_3$ nanowires on the graphene. It can be seen that $AgVO_3$ nanowires occupy most available surface area of graphene, giving much higher loadings of $AgVO_3$ nanowires in the composite aerogels, in which $AgVO_3$ nanowires have diameters of about 50 nm. We also found that some Ag particles are randomly distributed in the composite, which had already been reported in our previous work and other literatures.[14,20,21] The precipitation of Ag particles shrunk the structure cell of $AgVO_3$, hence making XRD main peak shifting to larger degree (Fig. S3). However, after enhanced post treatment temperature, all peaks can be readily indexed to the monoclinic β-$AgVO_3$ (JCPDS card no. 29-1154), due to most of Ag particles coming back to the structure cell. The lattice fringes of $AgVO_3$ nanowires were verified by HRTEM measurement. Fig. 2g shows a d-spacing of 0.273 nm that corresponds to the (-411) lattice plane of monoclinic β-$AgVO_3$ (JCPDS card no. 29-1154). Raman spectroscopy reveals that $AgVO_3$/GAs have the D-band around 1353 cm^{-1} and the G-band around 1596 cm^{-1}, exhibiting a ration of integrated peak intensities (I_D/I_G) of 1.034 (Fig. 2h). It is worth noting that the D and G band of $AgVO_3$/GAs exhibit a little bit blue-shift compared to that of pure graphene aerogels, which shall be attributed to the interactions between graphene and $AgVO_3$. X-ray photoelectron spectroscopy (XPS) shows that no peaks of other elements except C, O, Ag, and V are observed in the survey spectrum (Fig. S4), indicating the high purity of the composite aerogels.

The electrochemical performance of $AgVO_3$/GAs, where $AgVO_3$ nanowires account for 87 wt% in the composite, was firstly evaluated as cathode material of LIBs. Fig. 3a shows the cyclic voltammogram of $AgVO_3$/GAs electrode in the first five cycles in a potential range of 1.5 to 3.7 V *vs.* Li^+/Li at a scan rate of 0.1 mV s^{-1}. It can be seen that the five curves all keep the similar shapes and three apparent pairs of redox peaks. However, the peak intensity gradually decreases, and the potential differences between each redox process become smaller from the 1st to 5th cycle, suggesting the improved reversibility of Li^+ insertion/extraction with cycling. As for the fifth cycle, during the cathodic polarization process, three peaks are located at around 2.96, 2.55, and 1.76 V *vs.* Li^+/Li, corresponding to the complicated multistep electrochemical lithium intercalation processes; while in the following anodic polarization, three characteristic peaks are also observed at 3.33, 2.72, and 1.94 V, corresponding to the lithium deintercalation processes. As for the cathodic polarization process, we can easily index the three cathodic peaks to the corresponding reduction reactions. The peak at 2.96 V is assigned to silver reduction from Ag^+ to Ag^0, and the peak at 2.55 V corresponds to dominant reduction from V^{5+} to V^{4+} and partial reduction from V^{4+} to V^{3+}, whereas the peak at 1.76 V is in match with further reduction of vanadium from V^{4+} to V^{3+} and Ag^+ to Ag^0, all of which are similar to our previous work[20] and other reports[14].

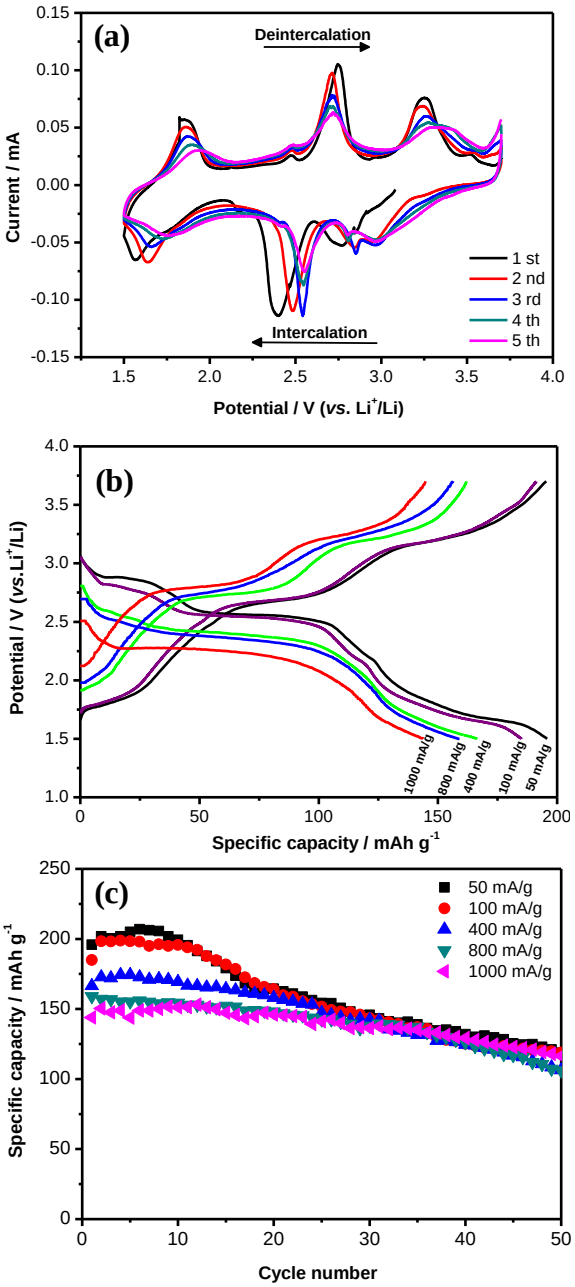

Fig. 3 (a) Cyclic voltammetry of $AgVO_3$/GAs at a scan rate of 0.1 mV s^{-1}. (b) The first cycle discharge-charge profiles of $AgVO_3$/GAs at various current densities from 50 to 1000 mA g^{-1}. (c) The cycling performance of the composite aerogels at various current densities.

Fig. 3b depicts the first discharge-charge profiles of $AgVO_3$/GAs at various current densities from 50 to 1000 mA g^{-1}. It is striking to note that high initial discharge capacities of about 195.8 mAh g^{-1} at 50 mA g^{-1}, 166.5 mAh g^{-1} at 400 mA g^{-1}, and

143.9 mAh g^{-1} up to 1000 mA g^{-1} were achieved for the composite aerogels electrode, and the capacity retention is as high as 73.5%. Although the first discharge capacities are not very high at small current densities of 50 and 100 mA g^{-1}, the capacities at large current densities of 400, 800 and 1000 mA g^{-1} are rather competitive than reported capacities.[22] The values show that $AgVO_3$/GAs has excellent rate capability, due to its unique 3D porous framework improving the electrical conductivity of $AgVO_3$ and allowing most of graphene sheets to be exposed to electrolyte. It is also found from the discharge curve at 50 mA g^{-1} that there are three discharge plates at 2.89, 2.56, and 1.78 V, which correspond to different lithium intercalation processes, respectively. And the results are in good match with the CV results (Fig. 3a).

As we mentioned in the introduction, $AgVO_3$ shows low electrical conductivity and slow Li^+ diffusion rate, resulting to poor cycling stability and rate capability as a cathode material for lithium-ion batteries. Therefore, a lot of work had already been conducted to improve its electrical conductivity and Li^+ diffusion rate, such as the combination with conductive polymer modification and the construction of nanosized materials.[18,19,21,23] However, the enhanced electrochemical properties are not very satisfactory. In this work, we tried to improve the cycling stability of $AgVO_3$ by adding graphene to build 3D composite aerogels structure.

The cycling stability of $AgVO_3$/GAs was investigated at different current densities. In Fig. 3c, the 50 th discharge capacities are 118.8, 118.9, 106.4, 106.1, and 116.4 mAh g^{-1} at current densities of 50, 100, 400, 800, 1000 mA g^{-1}, and the corresponding capacity retentions are 60.9%, 62.9%, 63.9%, 66.7%, and 80.9%, respectively. They are not only higher than the pure $AgVO_3$ nanowires in our previous work[20], but also are very high values among silver vanadium oxides (SVOs) electrodes that have been reported so far. For example, the capacity retentions of β-$AgVO_3$ nanowire clusters are around 41.2% and 43.6% after 50 cycles at current densities of 50 and 100 mA g^{-1}, respectively.[22] And more detailed comparisons can be found in Supporting information Table S1, suggesting that our $AgVO_3$/GAs show better cycling stability than those previously reported data. Noting the fact that the amount of graphene in composite aerogels could be not the optimal value, 3D composite aerogels with even better device performance are highly anticipated and now the related detailed investigation is ongoing in our group.

In summary, we have successfully synthesized 3D porous $AgVO_3$/graphene composite aerogels with high electrical conductivity and mechanical flexibility. The hybrid aerogels exhibit high discharge capacities, excellent rate capability, and good cycling stability for high-performance lithium ion storage, due to its improved electrical conductivity and fast charge transport that are all benefited from its 3D porous network. It is expected that this work can be used to develop other 1D nanomaterials in integration with 2D graphene nanosheets for creating more 3D composite aerogels with charming properties for various applications.

Acknowledgements

This work was financially supported by the National Nature Science Foundation of China (No. 51102010， 21336003, 21371021), 111 Project (No. B07004), the Fundamental Research Funds for the Central Universities (Grant No. ZZ1232), the Program for New Century Excellent Talents in University of China (NCET-12-0758), European Research Council Grant (ThreeDSurface) and BMBF (ZIK: 3DNanoDevice).

Notes and references

1 J. Sun, H. M. Liu, X. Chen, D. G. Evans, W. S. Yang and X. Duan, *Adv. Mater.*, 2013, **25**, 1124.

2 F. Liu, S. Y. Song, D. F. Xue and H. J. Zhang, *Adv. Mater.*, 2012, **24**, 1089.

3 Z. Xu, Y. Zhang, P. G. Li and C. Gao, *ACS Nano*, 2012, **6**, 7103.

4 J. H. Zou, J. H. Liu, A. S. Karakoti, A. Kumar, D. Joung, Q. Li, S. I. Khondaker, S. Seal and L. Zhai, *ACS Nano*, 2010, **4**, 7293.

5 M. A. Worsley, P. J. Pauzauskoe, T. Y. Olson, J. Biener, J. H. Satcher and T. F. Baumann, *J. Am. Chem. Soc.*, 2010, **132**, 14067.

6 H. P. Cong, X. C. Ren, P. Wang and S. H. Yu, *ACS Nano*, 2012, **6**, 2693.

7 H. Hu, Z. B. Zhao, W. B. Wan, Y.Gogotsi and J. S. Qiu, *Adv. Mater.*, 2013, **25**, 2219.

8 Z. Y. Sui, Q. H. Meng, X. T. Zhang, R. Ma and B. Cao, *J. Mater. Chem.*, 2012, **22**, 8767.

9 Z. S. Wu, A. Winter, L. Chen, Y. Sun, A. Turchanin, X. L. Feng and K. Müllen, *Adv. Mater.*, 2012, **24**, 5130.

10 Z.S. Wu, S. B. Yang, Y. Sun, K. Parvez. X. L. Feng and K. Müllen, *J. Am. Chem. Soc.*, 2012, **134**, 9082.

11 J. J. Yuan, J. W. Zhu, H. P. Bi, Z. Z. Zhang, S. Chen, S. M. Liang and X. Wang, *RSC Adv.*, 2013, **3**, 4400.

12 K. J. Takeuchi, A. C. Marschilok, S. M. Davis, R. A. Leising and E. S. Takeuchi, *Goord. Chem. Rev.*, 2001, **219-221**, 283.

13 K. J. Takeuchi, R. A. Leising, M. J. Palazzo, A. C. Marschilok and E. S. Takeuchi, *J. Power Sources*, 2003, **119-221**, 973.

14 S. Y. Zhang, W. Y. Li, C. S. Li and J. Chen, *J. Phys. Chem. B*, 2006, **110**, 24855.

15 J. W. Lee and B. N. Popov, *J. Power Sources*, 2006, **161**,565.

16 R. A. Leising, W. C. Thiebolt and E. S. Takeuchi, *Inorg. Chem.*, 1994, **33**, 5733.

17 R. P. Ramasamy, C. Feger, T. Strange and B. N. Popov, *J. Appl. Electrochem.*, 2006, **36**, 487.

18 L. Q. Mai, X. Xu, C. H. Han, Y. Z. Luo, L. Xu, Y. M. Wu and Y. L. Zhao, *Nano Lett.*, 2011, **11**, 4992.

19 J. W. Lee and B. N. Popov, *J. Power Sources*, 2006, **161**, 565.

20 L. Y. Liang, H. M. Liu and W. S. Yang, *Nanoscale*, 2013, **5**, 1026.

21 Z. J. Chen, S. K. Gao, R. H. Li, M. D. Wei, K. M. Wei and H. S. Zhou, *Electrochim. Acta*, 2008, **53**, 8134.

22 C. H. Han, Y. Q. Pi, Q. Y. An, L. Q. Mai, J. L. Xie, X. Xu, L. Xu, Y. L. Zhao, C. J. Niu, A. M. Khan and X. Y. He, *Nano Lett.*, 2012, **12**, 4668.

23 Y. Z. Wu, P. N. Zhu, X. Zhao, M. V. Reddy, S. J. Peng, B. V. R. Chowdari and S. Ramakrishna, *J. Mater. Chem. A*, 2013, 1, 852.